Recovering 3D+t scenes from 3D and 2D+t data by motion compensation and using a prior surface model.

Wafa Rekik, Dominique Béréziat, Séverine Dubuisson

Research report LIP6

Recovering 3D+t scenes from 3D and 2D+t data by motion compensation and using a prior surface model.

Reconstruction de scènes 3D+t à partir de données 2D+t par compensation du mouvement sur un modèle de surface.

Wafa Rekik[1], Dominique Bérézia[2,3], Séverine Dubuisson[2].

September 2010

[1]Present address: wafa.rekik@gmail.fr
[2]Department LIP6, Université Pierre et Marie Curie, 4 place Jussieu 75004, Paris, France.
[3]Corresponding author at: UPMC 4, place Jussieu 75004, Paris, France; tel: +33 1 44 27 47 71; fax: +33 1 44 27 53 53; mail: dominique.bereziat@upmc.fr

Abstract

In this paper, we address 3D+t shape recovery from 3D spatial data and 2D+t temporal sequences. This reconstruction is particularly challenging due to the great deal of in-depth information loss observed on the 2D+t temporal sequence. To handle this critical lack of information, we use a geometrical local constraint defined by a spherical topology arising in number of computer vision applications. Our approach consists in gradual 2D-to-3D restoration by motion compensation using a brightness constancy constraint and a spatial regularity criterion. Data prior geometrical model implies that structures of interest evolve on a spherical support. Motion has then only two degrees of liberty. We build then an adapted 2D model in the surface domain, where movement assumptions are more relevant, using a spherical parametrization. We restore 2D+t surfaces parametrized by spherical angular coordinates that we display using an adapted visualization tool.

Keywords

3D+t reconstruction, optical flow, spherical parametrisation.

Résumé

Le problème de la reconstruction de formes 3D en temps à partir d'une séquence d'images 2D et d'une image 3D statique est abordé. Ce problème est difficile en raison de la perte d'information de profondeur engendrée par le procédé 2D d'acquisition des images. Ce manque d'information est compensé par l'utilisation d'une contrainte géométrique induite par la topologie sphérique des objets rencontrés dans certaines images issues de l'imagerie biologique. Nous procédons par compensation du motion entre l'image 3D reconstruite au temps précédant et l'image 2D observé au moyen d'une équation 2D de transport de la luminosité. Le modèle est paramétrisé en coordonnées sphériques ce qui permet de formuler le problème en 2D. Les surfaces ainsi reconstruites sont visualisées en utilisant un outil de visualisation adapté.

Mots clés

Reconstruction 3D+t, flot opique, paramétrisation sphérique.

1 Introduction

In some computer vision applications, we deal with volumetric, *i.e.* 3D, acquisitions framing temporal, *i.e.* 2D+t, ones (Fig. 1). First type of acquisitions provides a description of the 3D scene geometry, thus, purely spatial information. Second ones observes 2D object motion providing temporal and partial spatial information. A possible approach to mine exhaustively these complementary datasets is to carry out a complete spatio-temporal or a 3D+t scene reconstruction. 3D+t sequences are restored by recovering the 3D original volume from each 2D frame belonging to the 2D+t sequence.

As the matter of fact, 3D reconstruction is an inverse problem. In this particular case, it is also an ill-posed problem since a single 2D frame is hardly sufficient to recover the 3D original

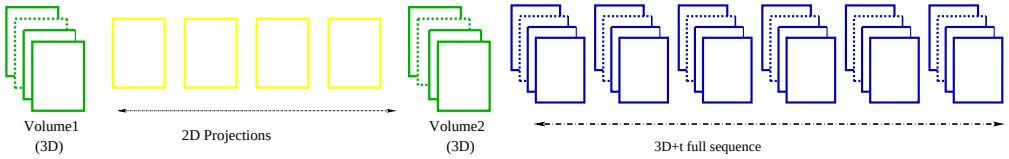

Figure 1: Recovering a 3D+t sequence from a couple of 3D images framing a series of 2D projections.

volume. Indeed, this frame exhibits a great deal of spatial distortions and in-depth loss of information caused by the projective transformation that reduces the 3D real structure into a 2D image. To handle this critical lack of information, we introduce a prior data model. It consists in a geometrical constraint defined on a spherical topology. Data observing locally spheric shaped objects can be issued from remote sensing acquisitions and especially in meteorology, from astronomical ones focusing on the Sun and in bio-cellular microscopic imagery. A relevant biologic application is described in [9] where biologists study dynamic of structures of interest evolving on a spherical cell simulation surface. In this context, for instance, spatial datasets consist in multi-focus acquisitions. Hence, they are not actual 3D images since they are formed by a series of equal sized slices, where signal in each slice is bothered by luminosity coming from adjacent ones. A spatial deconvolution stage is therefore needed when biologists calibrate correctly the video microscopy system to cell wall simulation experiments. Due to this limitation and to respect generality, we use synthetic data to validate our algorithm.
Our approach uses this geometrical prior constraint in order to select a relevant reconstruction strategy. In the context of locally spheric shaped data, the information of interest is embedded on the outer curved surface. This allows the 3D-to-2D transformation to be modeled simply with a surface based reconstruction approach. On one hand, inverse 3D restoration is performed gradually by motion compensation involving a spatial regularity criterion that balances the in-depth loss of information. On the other hand, since movement has only two angular degrees of liberty, we opt for a spherical parametrisation to investigate motion in the surface domain instead of building a 3D model. For the latter, computation of spatial derivatives is incoherent and noisy, mainly with reference to the normal to the surface. Besides movement constraints are not relevant. We restore then spherical surfaces, parameterized by angular coordinates, that we display directly by an adapted visualisation tool, called MAPVIS [8].

2 State-of-the-art

In the literature, a wide scope of approaches addresses the 3D reconstruction problem. Volume based methods aim at restoring an accurate description of luminosity in each voxel of the 3D reconstructed image, while surface based ones provide a 3D model of the object of interest. This model requires shape and texture recovery of the outer visible side of the observed object. Namely, tomographic reconstruction [7] focuses on restoring the original volume from multiple projective views. Stereo-vision [4] approaches make use in general of the triangulation principle in order to recover the surface shape of selected targets. Moreover, 2D-to-3D registration methods re-

construct 3D features from only one projective view. This registration consists in identifying a geometrical transformation that aligns 2D frames with 3D datasets often issued from a different modality of acquisition. This alignment determines their relative position and orientation and then locates them in the coordinate system of the 3D images. It is of growing interest in the medical imaging field mainly to register 3D pre-operative images (like MRI or CT images) into 2D series of intra-operative frames acquired during a surgical intervention. Registration may operate on feature-based methods or intensity based ones. Reader is referred to [2, 6]. Tomography and stereovison, namely, require multiple projective views to achieve the reconstruction task. Therefore, approaches aligning 2D projection images to 3D datasets appear to be adapted to the context of our study. However these approaches fit into a registration framework rather than a reconstruction one, unless other projective views are available, which is quite unusual. They can be used alternatively for a preprocessing stage for some aforementioned applications. We then build an adapted reconstruction model involving a prior geometrical constraint.

3 Reconstruction by motion compensation

Our approach is based on the existence and the knowledge of a functional p that reduces every volumetric structure at each instant into a 2D frame. The central idea is to carry out the 3D+t reconstruction using a couple of 3D data acquired at two different instants as well as the 2D+t sequence acquired meanwhile. Since the intermediary video sequence presents an interesting temporal resolution, we propose to restore the underlying 3D structure of each of its frame. The latter provides only a partial description of the real 3D structure that we aim to estimate at a given instant t. We attempt to compensate this lack of information by the mean of a matching procedure with the 3D volumetric image estimated at $t-1$. For this purpose, we compute a displacement field matching both 3D structures. We introduce, consequently, a motion hypothesis expressing the assumption that a moving voxel keeps the same gray value over time. It is identical to the well known optical flow constraint [3]. It leads to a fundamental equation that we solve gradually in order to rebuild the whole 3D+t sequence, using the couple of 3D data as initial border conditions.

3.1 Modeling, assumptions

We carry out the 3D+t reconstruction using a series of 2D+t video sequence acquisitions intersected with 3D volumetric ones. We opt for the following notations for the remainder of the paper:

- $\mathbf{X}$ a 3D vector position, *i.e.* $\mathbf{X} = (x, y, z)$;
- $\mathbf{x}$ a 2D vector position, *i.e.* $\mathbf{x} = (x, y)$;
- $\mathbf{W}$ a 3D vector field, *i.e.* $\mathbf{W} = (u, v, w)$;
- $I(\mathbf{X}, t)$ a 3D+t sequence;
- $I_{2\text{D}}(\mathbf{x}, t)$ a 2D+t sequence;
- $\hat{I}(\mathbf{X}, t)$ the estimation of I at $(\mathbf{X}, t)$;

Concretely, we have two 3D structures at two different instants: $I^1 = I(\mathbf{X}, t_1)$ and $I^2 = I(\mathbf{X}, t_2)$. Between $t = t_1$ and $t = t_2$, we also dispose of a video sequence $I_{2\text{D}}(\mathbf{x}, t)$ describing all the 2D reductions of the $I(\mathbf{X}, t)$ structures evolving in this duration. Each 2D frame $I_{2\text{D}}$ is a projective sight, at a given instant t, of a 3D original volume. This projection only depends on the data acquisition mechanism. We model it by a linear and stationary transformation, called projection p, given by:

$$p(I)(x, y) = \int_{\mathbb{R}} I(x, y, z)h(z)dz, \tag{1}$$

where $h(z)$ is a function describing the interaction between observed objects and the input light signal. p integrates contributions of all 3D slices to produce a unique 2D image. It introduces then an important loss of information in the $z-$direction. In order to reconstruct gradually the 3D+t sequence, we estimate the 3D structure at a given instant t, using the data $I_{2\text{D}}(\mathbf{x}, t)$ extracted from the 2D+t sequence. We then minimize the discrepancy between $p(\hat{I})$ and $I_{2\text{D}}$. A straightforward data model equation is:

$$p(\hat{I})(\mathbf{x}, t) - I_{2\text{D}}(\mathbf{x}, t) = 0, \ \forall t \in [t_1, t_2] \tag{2}$$

Since objects of interest evolve slowly from t to $t-1$, we can match $\hat{I}(\mathbf{X}, t)$ with the 3D structure $I(\mathbf{X}, t-1)$ known at the previous instant. This matching is quantified in terms of a displacement vector field $\mathbf{W}$ between both images. It expresses the assumption that a moving voxel keeps the same gray value over time yielding the following motion constraint, similar to optical flow one:

$$\hat{I}(\mathbf{X}, t) = I(\mathbf{X} + \mathbf{W}, t-1) \tag{3}$$

We estimate a retrogress vector field defining voxel displacement from $t-1$ to t for notation conveniences (we represent $-\mathbf{W}$ in Section 4). Expanding the left-hand side of Equation (3) in a first order Taylor series leads to:

$$\hat{I}(\mathbf{X}, t) = \nabla I(\mathbf{X}, t-1).\mathbf{W} + I(\mathbf{X}, t-1), \tag{4}$$

where $\nabla = (\frac{\partial}{\partial x}, \frac{\partial}{\partial y}, \frac{\partial}{\partial z})$ is the gradient operator. Since p is a linear operator, injection of the Equation (4) in the earlier data model constraint (2) provides the 2D data motion constraint related to $\mathbf{W}$:

$$p(\nabla I(\mathbf{X}, t-1).\mathbf{W}) + p(I(\mathbf{X}, t-1)) - I_{2\text{D}} = 0 \tag{5}$$

We compute the velocity vector field $\mathbf{W}$ at each instant t.

3.2 Formulation in the spherical context

Let us point out that, in the context of spherical shaped data observations, structures of interest evolve on the surface of a ball of constant ray. Even-though the support is embedded on a 3D-space, movement has only two degrees of liberty. It is then relevant to estimate the vector field using a spherical surface parametrisation. Let's establish equations formulated in the previous section in the spherical context. For this purpose, we introduce two 2D images I^s and $I^s_{2\text{D}}$ defined by the following substitutions (see Fig. 2):

$$I^s(\theta, \varphi, t) = I(x(\theta, \varphi), y(\theta, \varphi), z(\theta, \varphi), t) \tag{6}$$

$$I^s_{2\text{D}}(\theta, \varphi, t) = I_{2\text{D}}(x(\theta, \varphi), y(\theta, \varphi), t) \tag{7}$$

with the following parametrisation:

$$\begin{aligned} x(\theta,\varphi) &= R\cos(\varphi)\sin(\theta) \\ y(\theta,\varphi) &= R\sin(\varphi)\sin(\theta) \\ z(\theta,\varphi) &= R\cos(\theta) \end{aligned}$$

The spherical coordinates φ and θ respectively stand for the longitude and co-latitude angles. Equation (6) expresses merely passage from cartesian coordinates to spherical ones. Equation (7) involves the mapping of the 2D frame texture into a hemisphere with same diameter that the 3D known balls. Data model constraint (2) becomes:

$$p(\hat{I}^s)(\theta,\varphi,t) - I^s_{2D}(\theta,\varphi,t) = 0 \tag{8}$$

Let's now set up p in the sphere reference mark schemed in Fig. 2. Operator p integrates, in a plane including both geographical poles, contributions of frontal and dorsal hemispheres.

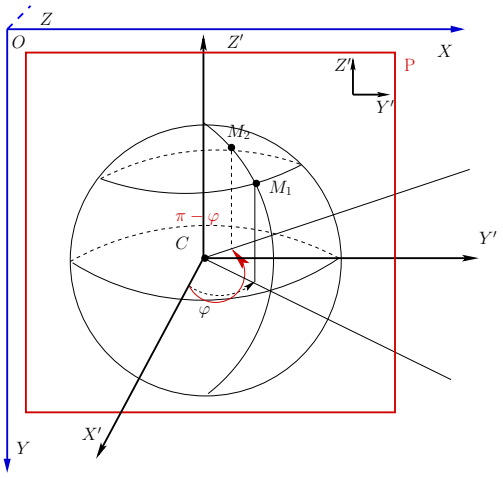

Figure 2: System of spherical coordinates. The projection plane corresponding to p is $P = (C, Y', Z')$.

Assuming that frontal and dorsal interactions with the input light signal are the same, p is defined by:

$$p(I^s)(\theta,\varphi) = I^s(\theta,\varphi) + I^s(\theta,\pi-\varphi) \tag{9}$$

Matching between $\hat{I}^s(.,t)$ and $I^s(.,t-1)$ are now expressed as performed in the cartesian parametrisation by Equation (3). According to Fig. 2 notations, the position of a moving point on the spherical surface is determined by the couple of angles (θ,φ) and the following equality : $\overrightarrow{CM} = R\overrightarrow{e_r}$,

where R is the sphere radius and $(\overrightarrow{e_r}, \overrightarrow{e_\theta}, \overrightarrow{e_\varphi})$ the Frenet local coordinate system related to M. Thus:

$$\hat{I}^s(R\overrightarrow{e_r}, t) = I^s(R\overrightarrow{e_r} + \partial R\overrightarrow{e_r}, t-1), \tag{10}$$

where $\overrightarrow{e_r} + \partial R\overrightarrow{e_r}$ is the elementary displacement at $R\overrightarrow{e_r}$ after the duration ∂t. Since R is constant, $\partial\overrightarrow{e_r}$ is defined by :

$$\partial\overrightarrow{e_r} = \partial\theta\partial\overrightarrow{e_\theta} + \sin(\theta)\partial\varphi\partial\overrightarrow{e_\varphi} \tag{11}$$

Inserting right-hand side of Equation (11) in the equality (10) leads to, for a unit sphere ($R = 1$):

$$\hat{I}^s(\overrightarrow{e_r}, t) = I^s(\overrightarrow{e_r} + \partial\theta\partial\overrightarrow{e_\theta} + \sin(\theta)\partial\varphi\partial\overrightarrow{e_\varphi}, t-1) \tag{12}$$

The right member of Equation (12) is linearized using a first order Taylor expansion. It yields the following equation:

$$\begin{aligned}\hat{I}^s(\theta,\varphi,t) = I^s_{t-1}(\theta,\varphi,t-1) + \frac{\partial I^s(\theta,\varphi,t-1)}{\partial\theta}\frac{\partial\theta}{\partial t} \\ + \sin(\theta)\frac{\partial I^s(\theta,\varphi,t-1)}{\partial\varphi}\frac{\partial\varphi}{\partial t}\end{aligned} \tag{13}$$

Inserting second member of Equation (13) in (8) and using linearity of the transformation p leads to:

$$\begin{aligned}p\Big(\frac{\partial I^s(.,t-1)}{\partial\theta}\frac{\partial\theta}{\partial t} + \sin(\theta)\frac{\partial I^s(.,t-1)}{\partial\varphi}\frac{\partial\varphi}{\partial t}\Big)(\theta,\varphi) \\ + \underbrace{p(I^s)(\theta,\varphi,t-1) - I^s_{2\mathrm{D}}(\theta,\varphi,t)}_{I'^s_{2\mathrm{D}}} = 0\end{aligned} \tag{14}$$

Finally, the data model constraint in the spherical context is:

$$p\Big(\frac{\partial I^s(.,t-1)}{\partial\theta}\frac{\partial\theta}{\partial t} + \sin(\theta)\frac{\partial I^s(.,t-1)}{\partial\varphi}\frac{\partial\varphi}{\partial t}\Big) + I'^s_{2\mathrm{D}} = 0 \tag{15}$$

3.3 Numerical Resolution

We compute an angular velocity field defined by the couple of angular variations $(\dot{\theta}, \dot{\varphi})$:

$$\left\{\begin{array}{rcl}\dot{\theta} & = & \frac{\partial\theta}{\partial t} \\ \dot{\varphi} & = & \frac{\partial\varphi}{\partial t}\end{array}\right. \tag{16}$$

For this sake, we have to solve the motion constraint given in (15). Let us introduce the aforementioned p expression in Equation (15):

$$\begin{aligned} p\Big(\frac{\partial I^s(.,t-1)}{\partial\theta}\frac{\partial\theta}{\partial t}+\sin(\theta)\frac{\partial I^s(.,t-1)}{\partial\varphi}\frac{\partial\varphi}{\partial t}\Big)= \\ \frac{\partial I^s(\theta,\varphi,t)}{\partial\theta}\dot{\theta}(\theta,\varphi)+\frac{\partial I^s(\theta,\pi-\varphi,t-1)}{\partial\theta}\dot{\theta}(\theta,\pi-\varphi)+ \\ \sin(\theta)(\frac{\partial I^s(\theta,\varphi,t-1)}{\partial\varphi}\dot{\varphi}(\theta,\varphi)+ \\ \frac{\partial I^s(\theta,\pi-\varphi,t-1)}{\partial\varphi}\dot{\varphi}(\theta,\pi-\varphi)) \end{aligned} \tag{17}$$

where $(\dot{\theta}(\theta,\varphi),\dot{\varphi}(\theta,\varphi))$ is the couple of angular velocity fields on the frontal hemisphere and $(\dot{\theta}(\theta,\pi-\varphi),\dot{\varphi}(\theta,\pi-\varphi))$ the couple of fields on the dorsal one. Equation (15) involves four velocity fields. This is due to the transformation p that introduces a positioning ambiguity. Indeed, it is not possible to undoubtedly state if the original position of a given point on the projection plane is in the frontal or the dorsal hemisphere. In order to reduce variable space, we suppose that these velocity fields are related. Let's express relation between velocity fields on the frontal as well as on the dorsal hemisphere. This relation takes into account possible object occlusions. In fact, objects with same latitude and a double-quadrant adjusted longitude are mapped at exactly the same position in the projection plane (see Fig. 3). To circumvent this ambiguity of positioning, we assume that:

$$\left\{\begin{array}{lcl} \dot{\theta}(\theta,\pi-\varphi) & = & \dot{\theta}(\theta,\varphi) \\ \dot{\varphi}(\theta,\pi-\varphi) & = & -\dot{\varphi}(\theta,\varphi) \end{array}\right. \tag{18}$$

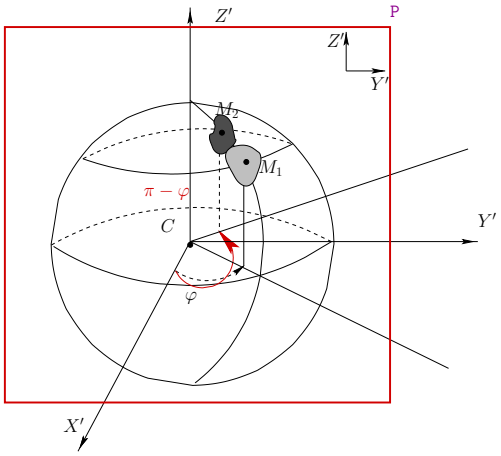

Figure 3: Occlusion of objects centered respectively in M_1 and M_2.

Under this assumption, number of variables is reduced to two. We estimate then velocities on the upper hemisphere, where θ has a range from 0 to π and φ from $-\frac{\pi}{2}$ to $\frac{\pi}{2}$. For the remainder of the globe, displacement vectors are issued from the system of equations (18). Data motion constraint is merely respect to $\mathbf{v} = (\dot{\theta}, \dot{\varphi})$:

$$\begin{aligned} \mathbb{M}(\mathbf{v})(\dot{\theta}, \dot{\varphi}, t) = p(\frac{\partial I^s(., t-1)}{\partial \theta})\dot{\theta} + \\ \sin(\theta)\big(\frac{\partial I^s(., t-1)}{\partial \varphi}(\theta, \varphi) - \frac{\partial I^s(., t-1)}{\partial \varphi}(\theta, \pi - \varphi)\big)\dot{\varphi} \\ + {I'}^s_{\text{2D}} = 0 \end{aligned} \tag{19}$$

Since this equation involves only two variables, we can build a bi-dimensional model to accurately recover motion. In order to estimate a dense motion field we use a variational formulation. We build a functional whose minimum, with respect to $\mathbf{v}$, corresponds to the solution of Equation (19):

$$E_1(\mathbf{v}) = \int_0^{\pi} \left(\int_{-\frac{\pi}{2}}^{\frac{\pi}{2}} \mathbb{M}(\mathbf{v})^2 d\varphi \right) d\theta$$

Since Equation (19) is under-determined, it is necessary to use an additional constraint to solve it. An obvious way is to constrain the spatial variations of $\mathbf{v}$ using a L_2 norm [11]. This regularization penalizes high spatial deformations of $\mathbf{v}$ and implicitly important variations with reference to the data known at a previous time:

$$E_2(\mathbf{v}) = \int_0^{\pi} \left(\int_{\frac{-\pi}{2}}^{\frac{\pi}{2}} \left(\|\nabla\dot{\theta}\|^2 + \|\nabla\dot{\varphi}\|^2 \right) d\varphi \right) d\theta$$

Other types of regularization may be used (L_1 norm, image driven norm, ...). Finally, our functional E, is, with respect to $\mathbf{v}$: $E = E_1 + \alpha E_2$, where α is a tuning parameter between the two terms that weights the importance of the regularization term E_2. Differentiation of E, with reference to $\dot{\theta}$ and $\dot{\varphi}$ yields a set of Euler-Lagrange equations [1]. Discretization of the latter with finite differences leads to a linear system, that we solve using a Gauss-Seidel iterative scheme.
Our goal, as schemed in Fig. 1, is to recover a full 3D+t sequence from the 2D+t series of data and the couple of 3D samples framing the temporal interval. The central idea is to estimate gradually velocity field between each 2D frame extracted from the 2D+t at a given instant t and the 3D structure previously estimated at $t-1$, as detailed in Section 3.1. Under the constant brightness assumption from time $t-1$ to t, an estimation of $\hat{I}^s(., t)$ is recovered from the data $I^s(., t-1)$ and angular variations $(\dot{\theta}, \dot{\varphi})$ by the following:

$$\hat{I}^s(\theta, \varphi) = I^s(\theta + \dot{\theta}, \varphi + \dot{\varphi}, t-1) \tag{20}$$

However angular coordinates $\theta + \dot{\theta}$ and $\varphi + \dot{\varphi}$, computed from discrete 2D couples, do not generally correspond to grid-positions in the output sampled image sequence I^s: they yield a set of scattered data. We attempt, therefore, to fit a smooth surface through the non-uniform distribution of these data samples. For this purpose, we represent our surface as a sum of weighted and shifted synthesis functions. B-splines stand apart for a good compromise between quality (namely high fidelity reconstruction and regularity) and computational issues, reader is referred to [10]. We then

use the method introduced in [5] and dedicated to recover such samples. The implemented algorithm makes use of a coarse-to-fine hierarchy of control lattices in order to generate a sequence of bi-cubic B-spline functions whose sum approaches the desired interpolation function.
In order to restore gradually the complete 3D+t sequence, we adopt a quite simple reconstruction strategy. We use, respectively, a forward progression procedure taking as first 3D available image, I^1 and a backward one using the final 3D available image I^2. Consequently, we generate two displacement vector fields at the median moment of the temporal interval $[t_1, t_2]$. The final 3D image is computed merely using the average of both fields. Let us point out that we restore surfaces parametrized by angular coordinates (θ, φ). To display results, we use an adapted visualisation tool called, MAPVIS [8], instead of carrying out inverse transformations in cartesian 3D+t grids. This tool displays complex information (scalar and vectorial) lying on real spheroid surfaces or projected ones. In the 3D case, MAPVIS projects data embedded on the actual globe observed part. Moreover, it improves visualisation of texture in perspective sight views of spheric shaped structures. This tool is based on a suitable planar map projection that unrolls the curved surface around a given origin. Therefore, varying the projection origin around the surface allows to observe different views of the sphere. Since the selected map projection minimizes distortions around the projection origin, the closer this point the more accurate the data recovery. Equatorial aspect of map projection, with reference to an origin lying on the equator displays the frontal hemisphere of the observed globe and polar one, with reference to the north geographical pole displays information lying on the northern hemisphere.

4 Results

We present, in this Section, a series of experiments in order to assess the performance of the proposed approach. They consist in computing the displacement vector field matching a 2D frame with an anterior 3D structure. As real data are not available, we have designed two sets of simple synthetic data. First one is composed of a couple of spheres $I(., t_1), I(., t_2)$ holding two squares lying on respectively the frontal and dorsal hemispheres. From t_1 to t_2, the frontal square center moves towards the right-bottom direction and the dorsal square evolves merely downwards. We simulate the 3D-to-2D transformation of $I(., t_2)$ yielding $I_{2\mathrm{D}}(., t_2)$ and we compute the spherical representation of I and $I_{2\mathrm{D}}$ using Equations (6,7). We then determine angular variation fields $(\dot{\theta}, \dot{\varphi})$ matching data $I^s(., t_1)$ with the projection $I^s_{2\mathrm{D}}(., t_2)$ in order to estimate $\hat{I}^s(., t_2)$ by motion compensation. Second set of data is quite identical to the first one, except that squares occlude each other in the 2D projection. Results are displayed in cartesian coordinates using MAPVIS. We display in Fig. 4 and 5 motion estimation results for respectively first and second set of synthetic data. Let us point out that motion computation produces a set of correct vector fields (from amplitude and direction point of views), perfectly tangent to the enclosing spherical surface. Moreover, our reconstruction method handles ambiguities, due to the 2D data position, by determining which hemisphere it is evolving in. It is noticeable by visualisation of the difference between the estimation of 3D image and the original one, *i.e.* $I(., t_2) - \hat{I}(., t_2)$. Performance of our algorithm is not bothered by the more complex case showing an object occlusion (see Fig. 5) which does not ease the aforementioned structure distinction problem. However image difference shows also reconstruction errors, doubtless amplified by the double interpolation procedure involved, first by the computation of a smooth surface from samples recovered by motion compensation, second by the

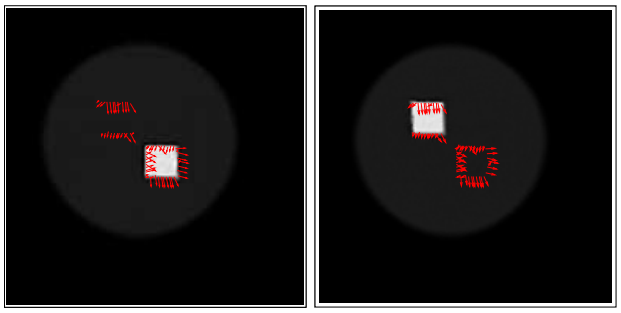

(a) From left to right: visualisation of the frontal then dorsal hemisphere of the set $(I(.,t_1), \mathbf{W})$.

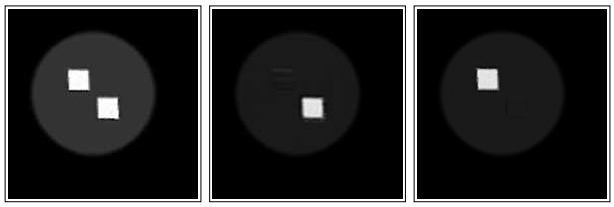

(b) From left to right: frontal view of projection $I_{2D}(.,t_2)$, frontal then dorsal hemisphere view of the estimated image $\hat{I}(.,t_2)$.

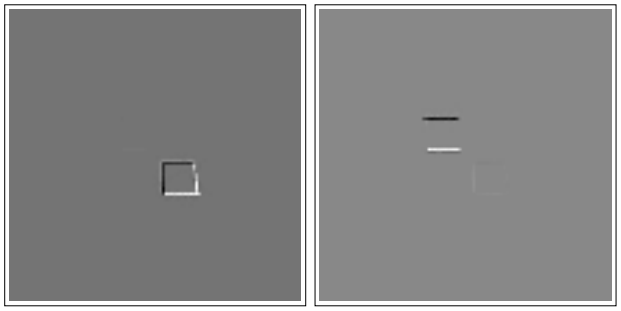

(c) From left to right: frontal then dorsal hemisphere view of the difference between original image and estimated one $I(.,t_2) - \hat{I}(.,t_2)$.

Figure 4: Result on sequence without occluding squares.

visualization of projective views [8]. These errors are localized in the border of moving objects. They may be caused by spatial derivative computations. Besides, they are due to the smoothing of motion discontinuities introduced by the spatial regularization of the estimated displacement vector field.

5 Conclusion

In this paper, we have presented an original approach dedicated to 3D+t scene reconstruction using 3D temporal data and 2D+t temporal sequences. It is based on motion compensation and involves a prior surface model. The latter concerns spherical topology arising in number of computer vision applications. In this context, structures of interest evolve on a spherical support. Although movement is embedded on a 3D domain, it has only two degrees of liberty. Consequently, it is more interesting to investigate motion in the surface domain than to build a 3D model. Consequently, we build a 2D model using a spherical parametrisation in order to compute angular velocity fields. Three dimensional spherical shapes are gradually restored by estimating angular variations. Matching is carried out under the assumption that a moving voxel keeps the same brightness over time. This assumption corresponds to the optical flow constancy constraint. Our approach recovers reliably the 3D structures and handles possible object occlusions. Thanks to the 2D modeling, implemented algorithms are not prohibitive compared to a full 3D approach. Moreover, we use an adapted tool, with relevant visualisation properties, in order to quickly display the restored surfaces parameterized by spherical angular coordinates. Currently, the whole sequence is computed frame by frame, causing errors cumulation along the sequence. This limitation could be circumvented using a spatio-temporal smoothness constraint computed globally on the whole sequence [12]. Discussing other reconstruction issues, it is possible to generalize the prior geometrical constraint to any regular surface. We propose also in another framework to solve the 3D+t scene recovery taken lower assumptions related to the data model. Moreover, we plan to apply our approach based on spherical topology to microscopic cell wall simulation acquisitions in the context described in [9]. That requires a spatial deconvolution framework to reconstruct each sphere from the original multi-focus image.

References

[1] R. Glowinski. *Numerical Methods for Nonlinear Variational Problems*. Series in computational physics. Springer, New York, 1984.

[2] A. Gueziec, P. Kazanzides, B. Williamson, and RH. Taylor. Anatomy-based registration of CT-scan and intraoperative X-ray images for guiding a surgical robot. *IEEE Trans Med Imaging*, 17:715–728, 1998.

[3] B.K.P. Horn and B.G. Schunk. Determining optical flow. *Artificial Intelligence*, 17:185–203, 1981.

[4] L. Huei-Yung. *Computer vision techniques for complete 3D model reconstruction*. PhD thesis, University of New York, 2002.

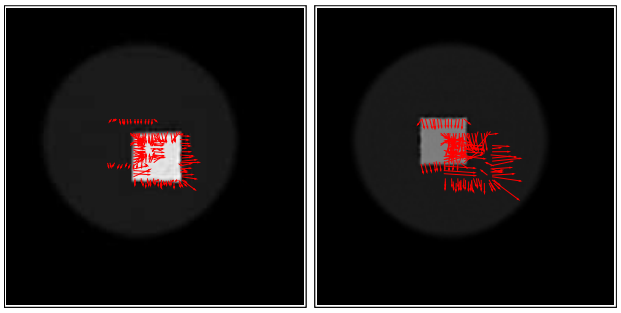

(a) From left to right: visualisation of the frontal then dorsal hemisphere of the set $I^s(.,t_1), \mathbf{W}$.

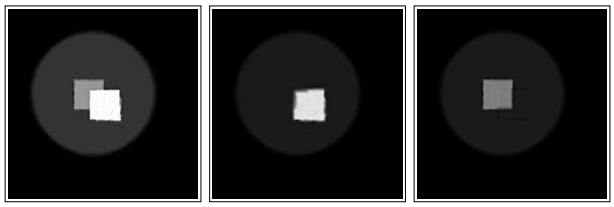

(b) From left to right: frontal view of projection $I_{2D}(.,t_2)$, frontal then dorsal hemisphere view of the estimated image $\hat{I}(.,t_2)$.

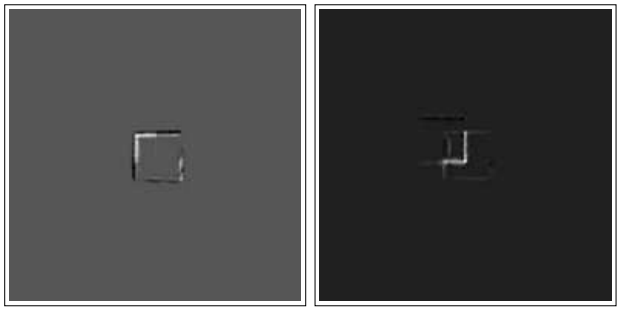

(c) From left to right: frontal then dorsal hemisphere of the difference between original image and estimated one $I(.,t_2) - \hat{I}(.,t_2)$.

Figure 5: Result on sequence with occluding squares.

[5] S. Lee, G. Wolberg, and S. Shin. Scattered data interpolation with multilevel B-splines. *IEEE Transactions on Visualization and Computer Graphics*, 3(3):228–244, July-September 1997.

[6] L. Lemieux, R. Jagoe, DR. Fish, ND. Kitchen, and DGt. Thomas. a patient-tocomputed-tomography image registration method based on digitally reconstructed radiographs. *Med Phys*, 21:1749–1760, 1994.

[7] F. Natterer. *The mathematics of computerized tomography*. Wiley, New York, 1986.

[8] W. Rekik, D. Béréziat, and S. Dubuisson. MAPVIS: a map-projection based tool for visualizing scalar and vectorial information lying on spheroidal surfaces. In *Proc. of IV05*, London, UK, July 2005.

[9] G. Staneva, M. Angelova, and K. Koumanov. Phospholipase A2 promotes raft budding and fission from giant liposomes. *Chem Phys Lipids*, 129:53–62, 2004.

[10] P. Thévenaz, T. Blu, and M. Unser. Image interpolation and resampling. In *Handbook of Medical Imaging*, volume 2, chapter 25, pages 393–420. Academic Press, 2000.

[11] A. Tikhonov. Regularization of incorrectly posed problems. *Sov. Math. Dokl.*, 4:1624–1627, 1963.

[12] J. Weickert and C. Schnorr. Variational optic flow computation with a spatio-temporal smoothness constraint. *Journal of Mathematical Imaging and Vision*, 14(3):245–255, May 2001.